Casimir effect mechanism of pairing between fermions in the vicinity of a magnetic quantum critical point

Yaroslav A. Kharkov and Oleg P. Sushkov
School of Physics, University of New South Wales, Sydney 2052, Australia
(Received 9 March 2015; revised manuscript received 21 April 2015; published 3 June 2015)

We consider two spin-1/2 fermions in a two-dimensional magnetic system that is close to the $O(3)$ magnetic quantum critical point (QCP) which separates magnetically ordered and disordered phases. Focusing on the disordered phase in the vicinity of the QCP, we demonstrate that the criticality results in a strong long-range attraction between the fermions, with potential $V(r) \propto -1/r^{\alpha}$, $\alpha \approx 0.75$, where r is the separation between the fermions. The mechanism of the enhanced attraction is similar to the Casimir effect and corresponds to multimagnon exchange processes between the fermions. While we consider a model system, the problem is originally motivated by the recent establishment of magnetic QCP in hole-doped cuprates under the superconducting dome at doping of about 10%. We suggest a mechanism of magnetic critical enhancement of pairing in cuprates.

DOI: 10.1103/PhysRevB.91.235105 PACS number(s): 74.40.Kb, 75.50.Ee, 74.20.Mn

I. INTRODUCTION

In the present paper, we study the interaction between fermions mediated by magnetic fluctuations in the vicinity of a magnetic quantum critical point. To address this generic problem, we consider a specific model of two holes injected into a bilayer antiferromagnet. The results presented below demonstrate that critical magnetic fluctuations lead to a long-range Coulomb-like attraction between the holes.

Our interest to this problem is motivated by cuprates. Lying at the center of the debate of high-T_c superconductivity is whether it originates from a Fermi liquid or from a Mott insulator. Recent experimental data, including angle-resolved photoemission spectroscopy (ARPES) support a Mott insulator scenario in underdoped cuprates and show a transition from small to large Fermi surface in the hole doping range $0.1 < x < 0.15$, see Refs. [1–3]. Magnetic quantum oscillations (MQO) in underdoped $YBa_2Cu_3O_{6+y}$ also support the small pocket scenario [4], in contrast to the large Fermi surface observed on the overdoped side [5]. Besides that, the existence of hole pockets is consistent with the picture of a dilute gas of holes dressed by spin fluctuations, based on doping a Mott insulator [6].

Optimally doped and overdoped cuprates do not have any static magnetic order. On the other hand, the underdoped cuprates possess a static incommensurate magnetic order at zero temperature. A magnetic QCP separating these two regions was predicted in Ref. [7] at doping $x \approx 0.1$. In $La_{2-x}Sr_xCuO_4$, the QCP is smeared out because of disorder. However, in $YBa_2Cu_3O_{6+y}$, the QCP is located experimentally with neutron scattering, nuclear magnetic resonance wipeout and muon spin rotation (μSR) at doping $x \approx 0.09$ ($y \approx 0.47$) [8–10]. At larger doping, after crossing the QCP, the (quasi-) static magnetic ordering vanishes and becomes fully dynamic.

It is widely believed that superconducting pairing in cuprates is driven by a magnetic mechanism. The most common approach is based on the spin-fermion model in the frame of normal Fermi liquid picture (large Fermi surface). Within this approach electrons interact via exchange of an antiferromagnetic (AF) fluctuation (paramagnon) [11]. The lightly doped AF Mott insulator approach, instead, necessarily implies small Fermi surface. In this case, holes interact/pair via exchange of the Goldstone magnon [12]. Due to the strong on-site Hubbard repulsion both approaches result in the d-wave pairing of fermions.

Magnetic criticality can significantly influence superconducting pairing. This idea has been recently considered by Wang and Chubukov [13] in the context of electron doped cuprates. There are also some earlier works referenced in Ref. [14]. However, to the best of our knowledge, all the previous works imply a normal liquid with a large Fermi surface. This might be a reconstructed Fermi surface which emulates small hole pockets [15], but still in essence this is a weak coupling normal Fermi liquid like approach. A large Fermi surface to a significant extent reduces the importance of the magnetic criticality for the pairing.

In this work, we consider two holes injected in the 2D "rigid" Mott insulator, so in essence our approach implies a small Fermi surface. Using a somewhat intuitive language, one can say that there are few holes in this regime and many more virtual magnons. In this case, the influence of the magnetic criticality on the coupling between two fermions is the most dramatic and the Casimir bag physics can fully manifest itself. As a Mott insulator host we use the bilayer antiferromagnet with magnetic fluctuations driven by the interlayer coupling. We consider the bilayer model for the sake of performing a controlled calculation. However, we believe that conceptually our conclusions are equally applicable to the single-layer and multilayer cuprates. The model presented here has only commensurate magnetic ordering, so we put aside incommensurability in cuprates.

The model under consideration demonstrates spin-charge separation at the QCP [16]. It means delocalization of hole spin due to dressing by a divergent magnon cloud. The effect of spin-charge separation points out to the nontriviality of the pairing problem. We are not aware of any other models of fermion pairing that incorporate the physics of spin-charge separation.

In order to probe the interaction between two fermions, we consider spin fluctuations in the system, keeping the fermions to be immobile and spatially localized, just as magnetic

impurities. In the very end of the paper, we argue that the mobility of fermions does not influence our conclusions, at least as soon as the fermion hopping amplitude is sufficiently small. Our calculations show that the single-magnon exchange becomes irrelevant close to the QCP. Instead, we obtain strong interfermion attraction in singlet and triplet spin channels due to the Casimir effect [17]. Each of the fermions (holes) builds up a "bag" of quantum magnetic fluctuations. The fermions attract each other, sharing a common bag and reducing the energy of the magnetic fluctuations inside of the bag. A "spin-bag" mechanism of attraction in the antiferromagnetic Neel phase was suggested by Schrieffer, Wen, and Zhang [18] in the context of high-T_c superconductivity. Another mechanism of Casimir magnetic attraction was proposed by Pryadko, Kivelson and Hone [19], but this suggestion is more a "van der Waals magnetic force" than a bag. Our model/mechanism is significantly different from previous suggestions, it is a real bag significantly based on the magnetic criticality. To make the semantics more clear, we underline the following points: (i) in the conventional single-magnon exchange mechanism, there is one magnon per two fermions; (ii) in the van der Waals like Casimir mechanism, there are two magnons per two fermions; and (iii) in the bag mechanism, there are very many magnons per two fermions. It is worth noting that the spin-bag model has conceptual similarity to QCD bag models for nucleon binding such as MIT [20] and chiral bags [21] that have being extensively studied from 1970's till now.

The structure of the paper is following. In Sec. II, we introduce a bilayer $J-J_\perp$ antiferromagnet, which is a simple but instructive model and contains all the essential physics of magnetic criticality. In Sec. II A, we characterize the magnetic quantum critical point driven by interlayer coupling $J_\perp/J$ and describe magnon excitations for an undoped AF in the disordered phase in the frame of spin-bond mean-field theory. Next, in Sec. II B, we move to the hole-doped $J-J_\perp$ model and show how holes interact with magnons. In Sec. III, which is the main content of the paper, we consider the hole-hole pairing problem at the QCP and show that pairing can not be described in terms of one-magnon exchange. In Sec. III A, we develop an effective theory for the Casimir interaction of the fermions, considering a double-fermion "atom," which can be either in a singlet or a triplet state. In Sec. III B, we present the results of solution to Dyson's equations for singlet and triplet Green's functions and finally show how the binding energy in both spin channels depends on the interfermion distance r. Finally, we draw our conclusions in Sec. IV and provide supplementary material in Appendix.

II. MODEL

Our model system is a $J-J_\perp$ square lattice bilayer Heisenberg antiferromagnet at zero temperature, where magnetic fluctuations are driven by interlayer coupling $J_\perp$ (see Fig. 1).

The Hamiltonian of the undoped host AF reads

$$H_{J,J_\perp} = J\sum_{\langle i,j\rangle}\left(\mathbf{S}_i^{(1)}\cdot\mathbf{S}_j^{(1)}+\mathbf{S}_i^{(2)}\cdot\mathbf{S}_j^{(2)}\right)+J_\perp\sum_i \mathbf{S}_i^{(1)}\cdot\mathbf{S}_i^{(2)}. \quad (1)$$

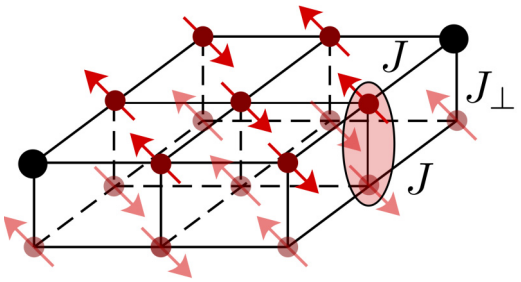

FIG. 1. (Color online) Bilayer $J-J_\perp$ antiferromagnet model. Two black dots on the top layer represent holes.

The superscripts (1) and (2) in Eq. (1) indicate the layers, $\langle i,j\rangle$ denotes summation over the nearest-neighbor sites. Here, $\mathbf{S}_i^{(1)}=\frac{1}{2}c^\dagger_{i\mu,1}\boldsymbol{\sigma}_{\mu\nu}c_{i\nu,1}$ is the spin of an electron at site i on the top plane and $c^\dagger_{i\sigma,1}/c_{i\sigma,1}$ is the creation/annihilation operator of an electron with spin $\sigma=\uparrow,\downarrow$ at site i, $\boldsymbol{\sigma}_{\mu\nu}$ are Pauli matrices. The Hamiltonian describes the antiferromagnetic coupling in each layer as well as between the two layers. It is known that without holes (half-filling) the model has an $O(3)$ magnetic QCP at $J_\perp/J=2.525$ (see Refs. [22–25]) separating the AF ordered and the magnetically disordered phase of spin dimers. Note that since we consider the zero-temperature case, the magnetic ordering in the AF phase is consistent with the Mermin-Wagner theorem. We dope the first layer with two holes. For simplicity, we set the hopping integrals equal to zero, therefore the holes are immobile. The holes interact with each other via magnetic fluctuations of the spins, i.e., exchanging by magnons.

In the subsections A and B of the current section, we will briefly present formalism that describes magnon excitations and hole-magnon interaction on the basis of the bilayer model. For more detailed explanations, see Ref. [16]; a reader which is not interested in these technical details can go directly to Sec. III.

A. Magnons at QCP

The magnetic excitations in the magnetically disordered phase are magnons, which are also called triplons in literature. In the present paper, we will use terms magnons and triplons as synonyms. To describe the magnons, we employ the spin-bond operator mean-field technique. This approach has been previously applied to quantum disordered systems such as bilayer antiferromagnets, spin chains, spin ladders, Kondo insulators, etc. [26–31]. It is known [27,28] that this simple technique gives the position of the QCP at $(J_\perp/J)_c\approx 2.31$, which is close to the exact value $(J_\perp/J)_c=2.525$ known from quantum Monte Carlo calculations [22,23], series expansions [24], and involved analytical calculations with the use of the Brueckner technique [25]. The spin-bond technique being much simpler than the Brueckner technique has sufficient accuracy for our purposes.

The bond-operator representation describes the system in a base of pairs of coupled spins on a rung, which can either be in a singlet or triplet (triplon) state. So, we define singlet $s_i^\dagger$ and triplet $(t_{ix}^\dagger,t_{iy}^\dagger,t_{iz}^\dagger)$ operators that create a state at site i with spin zero and spin one, which is polarized along one of

the axes (x,y,z). The four types of bosons obey the bosonic commutation relations. To restrict the physical states to either a singlet or triplet, the above operators are subjected to the constraint

$$s_i^\dagger s_i + \sum_\alpha t_{i\alpha}^\dagger t_{i\alpha} = 1. \tag{2}$$

In terms of these bosons, the spin operators in each layer $\mathbf{S}_i^{(1)}$ and $\mathbf{S}_i^{(2)}$ can be expressed as

$$S_{i\alpha}^{(1,2)} = \tfrac{1}{2}(\pm s_i^\dagger t_{i\alpha} \pm t_{i\alpha}^\dagger s_i - i\epsilon_{\alpha\beta\gamma} t_{i\beta}^\dagger t_{i\gamma}), \tag{3}$$

see Ref. [32]. Substituting the bond-operator representation of spins defined in Eq. (3) into the $H_{J,J_\perp}$ in Eq. (1), we obtain

$$\begin{aligned} H_{J,J_\perp} &= H_1 + H_2 + H_3 + H_4, \\ H_1 &= J_\perp \sum_i \left(-\frac{3}{4} s_i^\dagger s_i + \frac{1}{4} t_{i\alpha}^\dagger t_{i\alpha}\right), \\ H_2 &= \frac{J}{2} \sum_{\langle i,j\rangle} (s_i^\dagger s_j^\dagger t_{i\alpha} t_{j\alpha} + s_i^\dagger s_j t_{i\alpha} t_{j\alpha}^\dagger + \text{H.c.}), \\ H_3 &= \frac{J}{2} \sum_{\langle i,j\rangle} i\epsilon_{\alpha\beta\gamma} (t_{j\alpha}^\dagger t_{i\beta}^\dagger t_{i\gamma} s_j + \text{H.c.}), \\ H_4 &= \frac{J}{2} \sum_{\langle i,j\rangle} (t_{i\alpha}^\dagger t_{j\beta}^\dagger t_{i\beta} t_{j\alpha} - t_{i\alpha}^\dagger t_{j\alpha}^\dagger t_{i\beta} t_{j\beta}). \end{aligned} \tag{4}$$

The Hamiltonian (4) contains quadratic, cubic, and quartic terms in magnon operators t. The most important for us are the quadratic terms, because they provide quantum criticality. The only effect due to the nonlinear terms H_3 and H_4 is the renormalization of parameters near the QCP, such as the position of the QCP, magnon velocity, magnon gap, etc. This does not affect physics at the QCP, and therefore we will neglect these terms in further considerations.

The next step for treating the Hamiltonian (4) is to account for the hard-core constraint (2). It could be done by introducing an infinite on-site repulsion of triplons; however, this technique is quite involved. Another, more simple, way is to employ a mean-field approach, accounting for the constraint (2) via a Lagrange multiplier μ in the Hamiltonian:

$$H_{J,J_\perp} \to H_{J,J_\perp} - \mu \sum_i (s_i^\dagger s_i + t_{i\alpha}^\dagger t_{i\alpha} - 1). \tag{5}$$

Further analysis is straightforward. We replace singlet operators by numbers, $\langle s_i^\dagger \rangle = \langle s_i \rangle = \bar{s}$ (Bose-Einstein condensation of spin singlets), and diagonalize the quadratic in t Hamiltonian by performing the usual Fourier and Bogoliubov transformations:

$$t_{i\alpha} = \sqrt{\frac{1}{N}} \sum_{\boldsymbol{q}} e^{i\boldsymbol{q}\boldsymbol{r}_i} (u_q b_{q\alpha} + v_q b_{-q\alpha}^\dagger). \tag{6}$$

Here, N is the number of spin dimers in the lattice; the diagonalized Hamiltonian reads

$$H_m(\mu,\bar{s}) = E_0(\mu,\bar{s}) + \sum_{\boldsymbol{q}} \omega_q b_{q\alpha}^\dagger b_{q\alpha}, \tag{7}$$

where $\omega_q = \sqrt{A_q^2 - 4B_q^2}$ and coefficients $A_q = \frac{J_\perp}{4} - \mu + 2J\bar{s}^2\gamma_q$, $B_q = J\bar{s}^2\gamma_q$. Here, we define

$$\gamma_q = \tfrac{1}{2}[\cos(q_x) + \cos(q_y)]. \tag{8}$$

The lattice spacing is set to unity. The ground-state energy

$$E_0(\mu,\bar{s}) = N\left(-\frac{3J_\perp s^2}{4} - \mu\bar{s}^2 + \mu\right) + \frac{3}{2}\sum_{\boldsymbol{q}} (\omega_q - A_q) \tag{9}$$

just shifts the energy scale, and therefore is irrelevant for our purposes. The Bogoliubov coefficients u_q and v_q are given by

$$u_q = \sqrt{\frac{A_q}{2\omega_q} + \frac{1}{2}}, \quad v_q = -\text{sign}(B_q)\sqrt{\frac{A_q}{2\omega_q} - \frac{1}{2}}. \tag{10}$$

The parameters μ and $\bar{s}$ are determined by the saddle point equations: $\partial E_0(\mu,\bar{s})/\partial\mu = \partial E_0(\mu,\bar{s})/\partial\bar{s} = 0$. A solution to these equations gives the position of the QCP at $J_\perp/J = 2.31$ and values of "chemical potential" $\mu = -2.706$ and singlet density $\bar{s} = 0.906$. We see that even at the QCP, $\bar{s}$ is close to unity, which again justifies the smallness of the nonlinear terms H_3 and H_4 in the Hamiltonian.

The dispersion of magnons is

$$\omega_k = \sqrt{c^2(\mathbf{k} - \mathbf{Q})^2 + \Delta^2}, \quad \mathbf{Q} = (\pi,\pi) \tag{11}$$

in the vicinity of the wave-vector $\boldsymbol{Q}$, here, Δ is the magnon gap and c is the velocity of magnons $c = 2J\bar{s}^2 = 1.64J$, where the more precise value is $c = 1.9J$, see Ref. [24]. In the AF ordered phase, the magnons are Goldstone bosons and thus necessarily gapless. On the contrary, in the disordered phase, the gap opens up and the spin-bond approach gives $\Delta \propto (J_\perp - J_{\perp,c})$, which is not far from the prediction for $O(3)$ universality class systems $\Delta \propto (J_\perp - J_{\perp,c})^\nu$ with critical index $\nu = 0.71$ (see Ref. [33]). So, the spin-bond method provides a reasonably accurate description of the QCP.

B. Hole-magnon interaction

We dope our system with two immobile holes, by removing two electrons from the upper plane of the bilayer antiferromagnet. Hence we define the hole creation operator $a_{i\sigma}^\dagger$ with spin projection $\sigma = \uparrow,\downarrow$ by its action on the spin singlet bond $|s\rangle$:

$$a_{i\uparrow}^\dagger |s\rangle = c_{i\uparrow,2}^\dagger |0\rangle, \quad a_{i\downarrow}^\dagger |s\rangle = c_{i\downarrow,2}^\dagger |0\rangle, \tag{12}$$

where $|0\rangle$ is vacuum. The electron creation/annihilation operator in the upper plane can be expressed in terms of hole creation/annihilation operators $a_{i\sigma}^\dagger / a_{i\sigma}$ (see Ref. [29]), and after substitution in (1) it gives the following part of the Hamiltonian, which describes the hole-magnon interaction

$$\begin{aligned} H_{\text{hm}} = &-\frac{J\bar{s}}{2} \sum_{\langle i,j\rangle} \{(\mathbf{t}_j + \mathbf{t}_j^\dagger)\boldsymbol{\sigma}_i + (\mathbf{t}_i + \mathbf{t}_i^\dagger)\boldsymbol{\sigma}_j\} \\ &-\frac{J}{2} \sum_{\langle i,j\rangle} i(\boldsymbol{\sigma}_i[\mathbf{t}_j^\dagger \times \mathbf{t}_j] + \boldsymbol{\sigma}_j[\mathbf{t}_i^\dagger \times \mathbf{t}_i]). \end{aligned} \tag{13}$$

Here, $\boldsymbol{\sigma}_i = a_{i\mu}^\dagger \boldsymbol{\sigma}_{\mu\nu} a_{i\nu}$. The first line in the Hamiltonian (13) corresponds to the hole-magnon interaction vertex. The terms, describing a hole-double-magnon vertex, which come from the second line of (13) will be neglected below, because

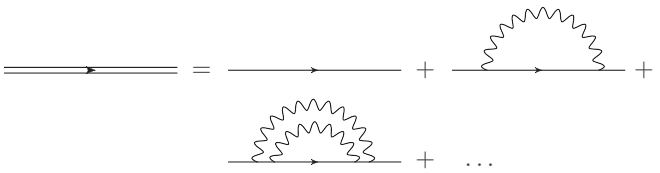

FIG. 2. Dyson's equation for single-hole Green's function in self-consistent Born approximation. Solid and wavy lines correspond to hole and magnon Green's functions.

they are irrelevant in the infrared limit, see next section for explanation of this point. Performing again standard Fourier and Bogoliubov transformations (6), the Hamiltonian (13) can be rewritten as

$$H_{\rm hm} \approx \sum_i \sigma_i^\alpha \sum_{\boldsymbol{q}} g_q (b_{q\alpha} e^{i\mathbf{q}\mathbf{r}_i} + b_{q\alpha}^\dagger e^{-i\mathbf{q}\mathbf{r}_i}). \tag{14}$$

The hole-magnon vertex is equal to

$$g_q = -\frac{J\bar{s}}{\sqrt{N}} \gamma_q (u_q + v_q). \tag{15}$$

Note that at the QCP the vertex diverges at $\mathbf{q} \to \mathbf{Q} = (\pi,\pi)$, because of the singularity of Bogoliubov coefficients $u_q, v_q \propto 1/\sqrt{\omega_q} \to \infty$.

The divergence of g_q is crucial for the physics of fermion-magnon coupling at the QCP. In fact, it results in the phenomenon of spin-charge separation for the single-fermion problem [16]. The spin of the hole is distributed in the power-law divergent cloud of magnons and, in this sense, is separated from the charge of the hole, localized on the hole's site. Later in the paper, we will show that the infrared divergence of the fermion-magnon coupling at the QCP results in strong power-law attraction between the fermions.

The importance of spin-charge separation for the single-fermion problem at the QCP could be seen from an analysis of the analytical structure of the hole Green's function. The standard approach in order to calculate one-fermion Green's function is to use $1/\mathcal{N}$ expansion for the $O(\mathcal{N})$ group, where $\mathcal{N} = 3$ is the number of magnon components. Summation of leading terms in the expansion arises in self-consistent Born approximation (SCBA), see Fig. 2.

Calculations of the hole Green's function in the disordered phase in SCBA have been performed in Refs. [34,35]. The results show that away from the QCP, in the disordered magnetic phase, the quasiparticle pole in the fermion Green's function is separated by Δ from the incoherent part of the Green's function. However, when approaching the QCP, the Green's function instead of the normal pole has just a branch cut singularity. This is a consequence of the infrared singularity of the coupling constant g_q.

The spectral density of the fermion Green's function (see Fig. 3) has inverse square root behavior

$$G(\epsilon) \propto 1/\sqrt{\epsilon_0 - \epsilon} \tag{16}$$

in the vicinity of the singularity point ϵ_0 and the quasiparticle residue is approaching zero, $Z \propto \sqrt{\Delta}$, at the QCP. Here,

$$\epsilon_0 \approx -0.97J \tag{17}$$

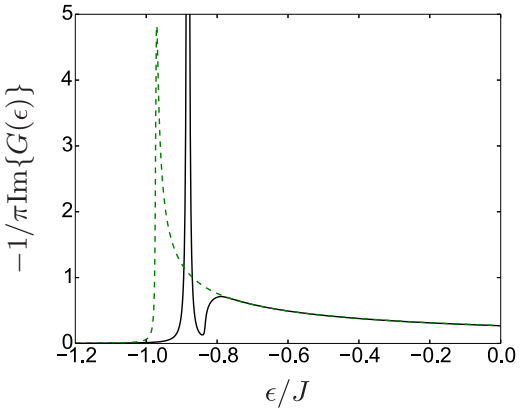

FIG. 3. (Color online) Spectral function $-1/\pi\ \mathrm{Im}[G(\epsilon)]$ of a single immobile hole obtained in SCBA (see Ref. [35]). The green dashed curve corresponds to the QCP ($\Delta = 0$), and the black solid line corresponds to the magnon gap $\Delta = 0.1J$. Note that at the QCP the quasiparticle pole disappears.

is the position of the branching point of the Green's function and has a meaning of fermion energy shift due to the interaction with magnons, where we set the bare energy of the hole to zero.

III. HOLE-HOLE INTERACTION, MEDIATED BY MAGNONS

Now we are ready to move to the actual problem of magnon mediated pairing of fermions and demonstrate new results. Adding up magnon Hamiltonian H_m, Eq. (7) and hole-magnon interaction Hamiltonian $H_{\rm hm}$, Eq. (14), we arrive to an effective Hamiltonian for two interacting holes, located at the sites with coordinates $\boldsymbol{r}_1$ and $\boldsymbol{r}_2$,

$$H_{\rm eff} = \sum_{\boldsymbol{q}} \omega_q b_{q\alpha}^\dagger b_{q\alpha} + \sum_{i=1,2} \sigma_i^\alpha \sum_{\boldsymbol{q}} g_q (b_{q\alpha} e^{i\boldsymbol{q}\boldsymbol{r}_i} + b_{q\alpha}^\dagger e^{-i\boldsymbol{q}\boldsymbol{r}_i}). \tag{18}$$

The Hamiltonian (18) is applicable only if the distance between holes $r = |\boldsymbol{r_1} - \boldsymbol{r_2}| > 1$, as long as we put aside direct exchange interaction between two neighboring holes.

The effective model (18) can be formulated in the language of a field theory. In fact, it is equivalent to the problem of two spin-1/2 fermions coupled to a vector field $\boldsymbol{\phi}(\boldsymbol{r})$, described by $O(3)$-symmetric theory with Lagrangian

$$\mathcal{L} = \frac{1}{2}(\partial_t \boldsymbol{\phi})^2 - \frac{c^2}{2}(\nabla \boldsymbol{\phi})^2 - \frac{\Delta^2}{2}\boldsymbol{\phi}^2 - \lambda(\boldsymbol{\phi}(\boldsymbol{r}_1)\boldsymbol{\sigma}_1 + \boldsymbol{\phi}(\boldsymbol{r}_2)\boldsymbol{\sigma}_2), \tag{19}$$

where λ is the coupling constant of fermion spin to magnon field. We focus only on the disordered magnetic phase, and therefore assume $\Delta^2 \geqslant 0$.

We would like to make three comments concerning the techniques and approximations we use in the present work. (i) We use SCBA as the main technical tool. The approximation is justified by the small parameter $1/\mathcal{N}$, where $\mathcal{N} = 3$, corresponding to the $O(3)$ symmetry group. Application of this method to the single-impurity problem [35] gives results extremely close to that obtained within the more conventional renormalization group approach [34]. (ii) We

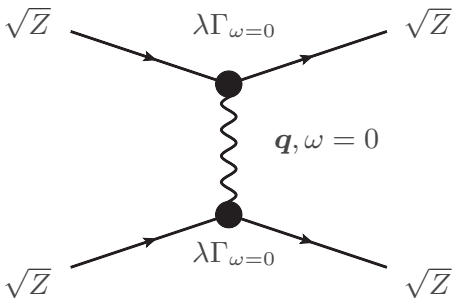

FIG. 4. One-magnon exchange diagram that provides a fermion-fermion interaction potential $V_{\rm int}^{(1)}(\boldsymbol{q})$. Note that the renormalization factor $\sqrt{Z}$ should be referred to each fermion line. Fermion-magnon vertices also come renormalized $\lambda \to \lambda\Gamma_{\omega=0}$.

neglected the self-action of magnons, the term $\propto \boldsymbol{\phi}^4$ is dropped in Eq. (19). There is no doubt that the self-action influences the position of the QCP, it also influences the critical index in the gap dependence, $\Delta \propto (J_\perp - J_{\perp,c})^\nu$. However, as soon as we express our answers in terms of Δ, the self-action is getting insignificant compared to the noncrossing diagrams accounted within SCBA. It can be illustrated by the single-impurity Green's function (16), the noncrossing diagrams dramatically reduce the fermion quasiparticle residue from $Z = 1$ to $Z \propto \Delta^{1/2}$, the anomalous dimension is $1/2$. On the other hand, the magnon self-action only slightly influences the magnon quasiparticle residue, $Z = 1 \to Z \propto \Delta^\eta$, the anomalous dimension is $\eta = 0.033$ [33]. (iii) We neglect the second line in the interaction (13). The simplest way to justify this is to use the field-theory language. In this language, the second line has the following kinematic form, $\boldsymbol{\sigma} \cdot [\boldsymbol{\phi} \times \partial_t \boldsymbol{\phi}]$. Because of the time derivative, the term is infrared irrelevant.

Parameters of the Lagrangian (19) could be directly expressed via parameters of the initial lattice Hamiltonian (1). As an example, the coupling constant λ in (19) is related to the hole-magnon vertex g_q in the effective Hamiltonian (18) as $g_q = \lambda/\sqrt{2\omega_q}$. Hence, for the Heisenberg bilayer model, $\lambda \approx 2J\sqrt{c}$. This equivalence shows that the problem of fermion pairing at the QCP, we are considering here, is generic. It has implications far beyond the particular bilayer model.

In order to calculate the pairing energy between two fermions, we first consider one magnon exchange contribution, Fig. 4. According to Feynman rules, we obtain the interaction potential

$$V_{\rm int}^{(1)}(\boldsymbol{q}) = -\lambda^2 Z^2 \Gamma_{\omega=0}^2 \frac{\langle \boldsymbol{\sigma}_1 \boldsymbol{\sigma}_2 \rangle}{c^2(\mathbf{q} - \mathbf{Q})^2 + \Delta^2}. \tag{20}$$

The factor Z^2 comes from $Z^{1/2}$ for each external fermion line. The vertex $\lambda\Gamma_{\omega=0}$ comes from diagrams in Fig. 5, $\lambda \to \lambda\Gamma_{\omega=0}$. Here, ω is the frequency of the exchange magnon, which is equal to zero. In the coordinate representation, the potential reads

$$V_{\rm int}^{(1)}(r) = -\frac{\lambda^2}{2\pi c^2} Z^2 \Gamma_{\omega=0}^2 \cos(\boldsymbol{Qr}) \langle \boldsymbol{\sigma}_1 \boldsymbol{\sigma}_2 \rangle K_0\left(\frac{r\Delta}{c}\right), \tag{21}$$

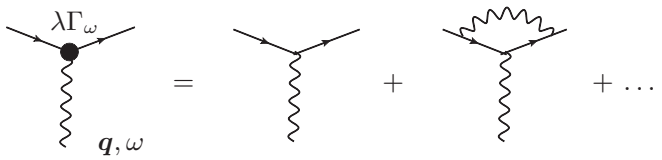

FIG. 5. The fermion-magnon vertex.

where K_0 is the Macdonald function of zeroth order. The potential energy $V_{\rm int}^{(1)}(r) \propto \ln(r)$ is logarithmic at small distances $r < c/\Delta$ and it exponentially decays at $r > c/\Delta$ as $V_{\rm int}^{(1)}(r) \propto e^{-r\Delta/c}$. The spin-dependent prefactor $\langle \boldsymbol{\sigma}_1 \boldsymbol{\sigma}_2 \rangle = 2[S(S+1) - 3/2]$ is determined by the total spin of two fermions S and equals to -3 in a singlet channel and $+1$ in a triplet channel. The potential is attractive in the state with a total spin zero (one) when

$$P_r = \cos(\boldsymbol{Qr}) = (-1)^{r_x + r_y} \tag{22}$$

is negative (positive) and repulsive in the opposite case ($\mathbf{r} = r_x \mathbf{e_x} + r_y \mathbf{e_y}$). This fact has clear physical meaning and reflects the AF character of spin correlations in the antiferromagnet. The system tends to restore AF ordering and the state when the spins of two interacting holes are aligned according to an antiferromagnetic pattern (see Fig. 6) is energetically preferable.

When we approach the QCP, the quasiparticle residue as well as the magnon-hole vertex tend to zero: $Z \propto \sqrt{\Delta} \to 0$ and $\Gamma_{\omega=0} \propto \Delta^{1/6} \to 0$ (see discussion in Sec. II B and Ref. [35]). Thus the single-magnon exchange contribution given by (21) vanishes, because the potential $V_{\rm int}^{(1)}$ is proportional to $Z^2\Gamma_{\omega=0}^2 \to 0$. Does this imply that pairing between fermions becomes very weak close to the QCP? Our answer is no, on the contrary, the pairing becomes very strong, but it is due to the Casimir bag mechanism.

Casimir effect attraction has different limits/regimes. The simplest one is the "van der Waals" regime, which is relevant to the van der Waals force between two neutral atoms. In this regime, the quasiparticle residue remains large, $Z \approx 1$, and the attraction is described by the box diagrams shown in Fig. 7; this approach to this effect was developed by Dzyaloshinsky [36]. The number of intermediate magnons is just two, it is equal to the number of fermions. The mechanism of Casimir magnetic attraction between impurities suggested in Ref. [19]

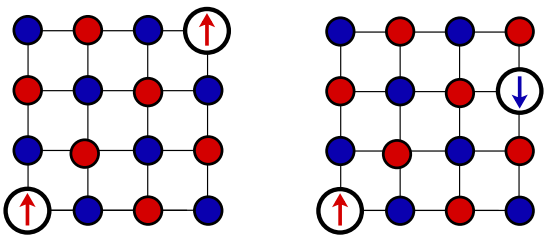

FIG. 6. (Color online) Dependence of spin channel, which provides attraction between holes on a mutual positioning of the holes in the lattice. Two holes with spins up symbolically represent a triplet channel, which provides negative interaction energy for $P_r = (-1)^{r_x + r_y} = +1$, two holes with opposite spins represent a singlet channel, which results in attraction when $P_r = -1$.

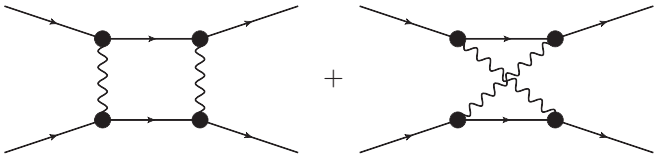

FIG. 7. The box diagrams for a two-magnon exchange between fermions. Note that the renormalization factor $\sqrt{Z}$ should be referred to each external fermion line.

for antiferromagnetically ordered phases belongs exactly to this regime. In this phase, the fermion's quasiparticle residue is practically unchanged due to the Adler's relation, and the attraction is described by simple box diagrams, see Ref. [37].

The diagrams in Figs. 4 and 7 contain $\sqrt{Z}$ per each external leg. While the presence of $\sqrt{Z}$ is a textbook statement [33], it is important to understand where it comes from. The origin is the quasiparticle description, these diagrams generate effective potentials/interactions between quasipraticles. As soon as the interaction is established, it is used in Schrodinger equation, Lippmann-Schwinger equation, or BCS equation. Obviously, the techniques based on the quasiparticle approach are not applicable in the case when $Z \to 0$ and the spectral weight becomes fully incoherent. To the best of our knowledge, the only known technique that does not refer to quasiparticles is Bethe-Salpeter equation (BSE), which operates with a two-fermion Green's function with amputated legs. Unfortunately, all known applications of BSE, for example, binding of positronium [38], in the end assume quasipraticles with nonzero residue. While, in principle, the BSE approach is applicable to our problem, all our attempts to apply the method were unsuccessful because of a large number of two-fermion irreducible diagrams with multiple magnon exchanges.

To solve the Casimir bag problem we have developed a diagramatic method, which we call the "Lamb-shift" technique. Similar to BSE in the Lamb-shift technique we also operate with a two-fermion Green's function. The advantage of BSE is that it is generic and in principle it is independent of the large parameter $\mathcal{N}$. On the other hand, the Lamb-shift technique is the large $\mathcal{N}$ expansion by construction. The advantage of the Lamb-shift technique is that it allows us to solve the multimagnon problem.

A. The Lamb-shift technique for calculation of Casimir interaction

In this section, we introduce a new technique to treat Casimir pairing energy. To incorporate "Casimir effect" physics, we consider a composite two-fermion "atom," which has total spin either zero (singlet state) or one (triplet state). Next, we calculate the Lamb shift in energy of this composite atom due to radiation of magnons as a function of separation between fermions.

Let us consider the effective theory for the composite object. The creation operator for a singlet state is

$$\Psi_S^\dagger = \frac{1}{\sqrt{2}}(a_{1\uparrow}^\dagger a_{2\downarrow}^\dagger - a_{1\downarrow}^\dagger a_{2\uparrow}^\dagger) \tag{23}$$

and for a triplet state

$$\begin{aligned}\Psi_{T,x}^\dagger &= \frac{-1}{\sqrt{2}}(a_{1\uparrow}^\dagger a_{2\uparrow}^\dagger - a_{1\downarrow}^\dagger a_{2\downarrow}^\dagger),\\ \Psi_{T,y}^\dagger &= \frac{i}{\sqrt{2}}(a_{1\uparrow}^\dagger a_{2\uparrow}^\dagger + a_{1\downarrow}^\dagger a_{2\downarrow}^\dagger),\\ \Psi_{T,z}^\dagger &= \frac{1}{\sqrt{2}}(a_{1\uparrow}^\dagger a_{2\downarrow}^\dagger + a_{1\downarrow}^\dagger a_{2\uparrow}^\dagger).\end{aligned} \tag{24}$$

According to the selection rules for interaction of the atom with a magnon, there are three types of transitions: $S \to T_\alpha$, $T_\alpha \to T_\beta$, and $T_\alpha \to S$, where S means singlet state and T_α denotes triplet state with polarization α. The only one invariant kinematic structure that provides coupling between S and T,α states with emission (absorption) of one magnon is $\{g_{ST}(q)\Psi_{T,\alpha}^\dagger \Psi_S(b_{q\alpha} + b_{q\alpha}^\dagger) + \text{H.c.}\}$. In a similar way, a transition of the type $T_\alpha \to T_\beta$ is governed by the term $ig_{TT}(q)\varepsilon_{\alpha\beta\gamma}\Psi_{T,\alpha}^\dagger \Psi_{T,\beta}(b_{q\gamma} + b_{q\gamma}^\dagger)$. The coefficients $g_{ST}(q)$ and $g_{TT}(q)$ are coupling constants for these transitions. Therefore the interaction of the two-fermion system with a magnon field in the singlet-triplet representation reads

$$\begin{aligned}\mathcal{H} = &\left[\delta_{\alpha\beta}\Psi_{T,\alpha}^\dagger \Psi_S \sum_{\boldsymbol{q}} g_{ST}(q)(b_{q\beta} + b_{q\beta}^\dagger) + \text{H.c.}\right]\\ &+ i\varepsilon_{\alpha\beta\gamma}\Psi_{T,\alpha}^\dagger \Psi_{T,\beta} \sum_{\boldsymbol{q}} g_{TT}(q)(b_{q\gamma} + b_{q\gamma}^\dagger).\end{aligned} \tag{25}$$

The effective vertices can be calculated by evaluating the matrix elements of the Hamiltonian (18) between states (23) and (24) :

$$\begin{aligned}g_{ST}(q) &= g_{TS}^*(q) = 2ig_q \sin\left(\frac{\boldsymbol{qr}}{2}\right),\\ g_{TT}(q) &= 2g_q \cos\left(\frac{\boldsymbol{qr}}{2}\right).\end{aligned} \tag{26}$$

Let us define the retarded Green's function for the singlet and triplet states:

$$\begin{aligned}G_{T,\alpha\beta}(t_2 - t_1) &= -i\langle 0|\Psi_{T,\beta}(t_2)\Psi_{T,\alpha}^\dagger(t_1)|0\rangle\theta(t_2 - t_1),\\ G_S(t_2 - t_1) &= -i\langle 0|\Psi_S(t_2)\Psi_S^\dagger(t_1)|0\rangle\theta(t_2 - t_1),\end{aligned} \tag{27}$$

where $|0\rangle$ is a ground state of the system and the theta function is

$$\theta(t) = \begin{cases}1, t > 0;\\ 0, t < 0.\end{cases} \tag{28}$$

Due to the $O(3)$ rotational invariance, the triplet Green's function should be of the form $G_{T,\alpha\beta}(t) = \delta_{\alpha\beta}G_T(t)$. Note that our definition of the Green's functions $G_S(t_2 - t_1)$, $G_T(t_2 - t_1)$ assumes that the fermions, which constitute the composite atom, are both created at the same moment of time t_1 and then both annihilated at the moment t_2. Apart from several other technical details, the creation/annihilation at the same time is the major difference of our technique from BSE. Fourier transform of Eq. (27) gives the Green's functions in

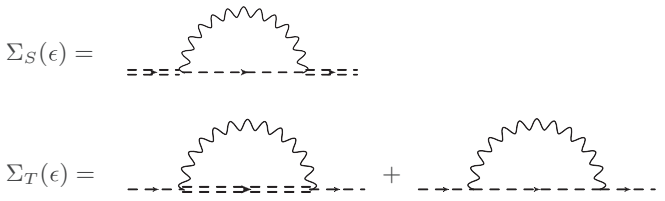

FIG. 8. Diagrams for singlet $\Sigma_S(\epsilon)$ and triplet $\Sigma_T(\epsilon)$ self-energies in SCBA. The double dashed line and dashed line represent a double-fermion Green's function in singlet and triplet channels, correspondingly. Analytical expressions for the diagrams are given in Eq. (31).

the frequency representation:

$$G_{S,T}(\epsilon) = \int_0^\infty dt e^{i(\epsilon+i0)t} G_{S,T}(t)\,. \tag{29}$$

The Dyson's equations for singlet and triplet state Green's functions read

$$G_{S,T}(\epsilon) = \frac{1}{\epsilon - \Sigma_{S,T}(\epsilon) + i0}. \tag{30}$$

We use SCBA to evaluate singlet and triplet self-energies:

$$\begin{aligned}\Sigma_S(\epsilon) =& 3\sum_{\boldsymbol{q}} |g_{ST}(q)|^2 G_T(\epsilon - \omega_q),\\ \Sigma_T(\epsilon) =& \sum_{\boldsymbol{q}} |g_{ST}(q)|^2 G_S(\epsilon - \omega_q)\\ &+ 2\sum_{\boldsymbol{q}} |g_{TT}(q)|^2 G_T(\epsilon - \omega_q).\end{aligned} \tag{31}$$

The diagrams for the singlet and triplet self-energies are presented in Fig. 8. The combinator factors here come from contraction of the corresponding tensor structures of the coupling vertices in (25) and have a meaning of the number of the polarizations of intermediate states.

Note that unlike the scattering amplitude (20), expressions (31) for the two-fermion self-energy do not contain single-fermion quasiparticle residues. Similar to the one-fermion problem, the residue of the composite atom Green's function is zero at the QCP. However, it is not a problem now, because we are interested only in the position of singularity of the Green's function, i.e., in two-fermion pairing energy.

Note also that the Dyson's equations (30) and (31) for the two-fermion system include processes when the fermions are dressed by magnons, as well as processes with (multi-)magnon exchanges between the fermions. Therefore the Lamb-shift approach implicitly accounts for the incoherent part of single-fermion Green's function, which is crucial in the vicinity of the QCP.

B. Solution to Dyson's equations for singlet and triplet states and hole-hole interaction energy

In order to find the interaction energy of two fermions, we numerically solve the system of two Dyson's equations (31) in the square Brillouin zone for different interfermion separations r, measured in units of lattice spacings. The energy grid in our computation is $\Delta\epsilon = 10^{-3}J$. The zero approximation Green's function is $G^{(0)}_{S,T}(\epsilon) = 1/(\epsilon + i0)$ and for artificial broadening we take $+i0 \to i10^{-3}J$. In order to perform numerical integration in Eq. (31), we can directly integrate over a square Brillouin zone, or introduce an effective momentum cutoff and integrate analytically over the angle in the momentum space and then integrate over the radial component of the momentum $|\boldsymbol{q}'| = |\boldsymbol{q} - \boldsymbol{Q}| \leqslant \Lambda_q \approx 1$ numerically. We have checked that there is a good agreement between these two methods. However, the effective momentum cutoff method is much more efficient for numerics and provides better precision of the computations, therefore we mostly used the later approach.

The limit $r \to \infty$ of infinite separation between the fermions corresponds to the case when the vertices in equations (31) are substituted by the averaged ones over q oscillations $|g_{ST}(q)|^2, |g_{TT}(q)|^2 \to 2|g_q|^2$. The position of the singularity of triplet and singlet Green's functions gives us the energy E_∞ of the two-fermion system separated by infinite distance. It is clear that in such limit the Green's functions in both spin channels should coincide $G_S(\epsilon) = G_T(\epsilon)$, which guarantees the same value for the asymptotic energy E_∞ in singlet and triplet states. So, we refer to the interaction energy as a difference $V_{\rm int}(r) = E(r) - E_\infty$.

We found that the value $E_\infty \approx -1.55J$ (at the QPC) is about 20% smaller compared to the doubled energy of an isolated single hole $2\epsilon_0 \approx -1.94J$, see Eq. (17). This difference is due to the fact that certain diagrams, which are presented in SCBA for a single-hole Green's function, are not included in SCBA for the two-hole Green's function $G_{S,T}$ (see Fig. 9). This deviation shows the precision of our method, which can be improved by calculating $1/\mathcal{N}$ corrections to SCBA (31).

As it is seen from the structure of effective vertices,

$$\begin{aligned}|g_{ST}(q)|^2 &= 2g_q^2(1 - P_r \cos \boldsymbol{q}'\boldsymbol{r}),\\ |g_{TT}(q)|^2 &= 2g_q^2(1 + P_r \cos \boldsymbol{q}'\boldsymbol{r}),\end{aligned} \tag{32}$$

the system's behavior greatly depends on the "parity" $P_r = (-1)^{r_x+r_y}$ of the interfermion distance. The holes prefer to form a singlet (triplet) spin state for negative (positive) parity P_r at given r.

First, let us consider the case, when the system is away from the QCP, $\Delta > 0$. We plot spectral functions

$$A_{S,T}(\epsilon) = -\frac{1}{\pi}\,\mathrm{Im}[G_{S,T}(\epsilon)] \tag{33}$$

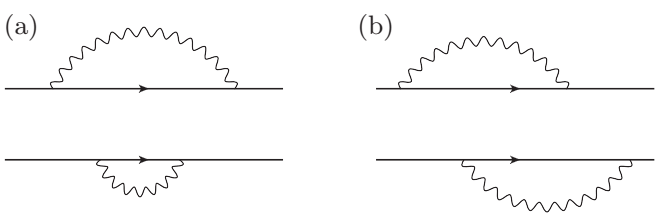

FIG. 9. Diagrams contributing to E_∞. Top and bottom solid lines correspond to a single-hole Green's function. Diagram (a) is accounted in SCBA (31), diagram (b) is not included in (31) and corresponds to the $1/\mathcal{N}$ correction to SCBA.

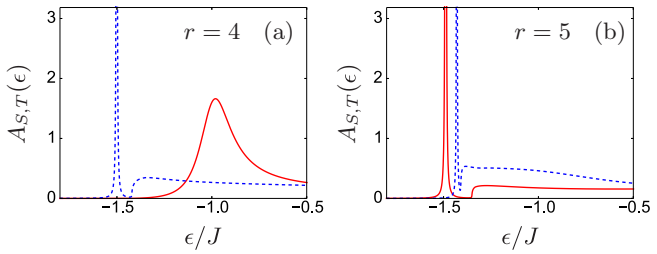

FIG. 10. (Color online) Spectral functions $A_S(\epsilon)$, $A_T(\epsilon)$ of double-fermion Green's functions in singlet and triplet channels close to the QCP ($\Delta = 0.08J$). (a) corresponds to interhole distance $r = 4$ and (b) corresponds to $r = 5$. Blue dashed lines correspond to a triplet state, red solid lines correspond to a singlet state.

for singlet and triplet Green's functions at different r, see Figs. 10(a) and 10(b).

We see a well defined quasiparticle peak in the triplet (singlet) spin channel at $r = 4$ ($r = 5$). However, in the opposite spin channel, the peak broadens and submerges to continuum. This effect can be interpreted as a formation of an excited decaying state, which is coupled via magnons to the ground state.

In Fig. 11, we plot the fermion-fermion interaction energy versus distance. The inset displays the interaction energy when the system is away from the QCP (the magnon gap is large, $\Delta = 0.67J$). Squares and triangles show results of our Lamb-shift technique calculations and solid lines represent the single-magnon exchange formula (21). There is an excellent agreement between the two approaches. The main part of Fig. 11 shows the same quantities, but close to the QCP (the magnon gap is small, $\Delta = 0.08J$). Here, we observe a dramatic disagreement between the result of the Lamb-shift

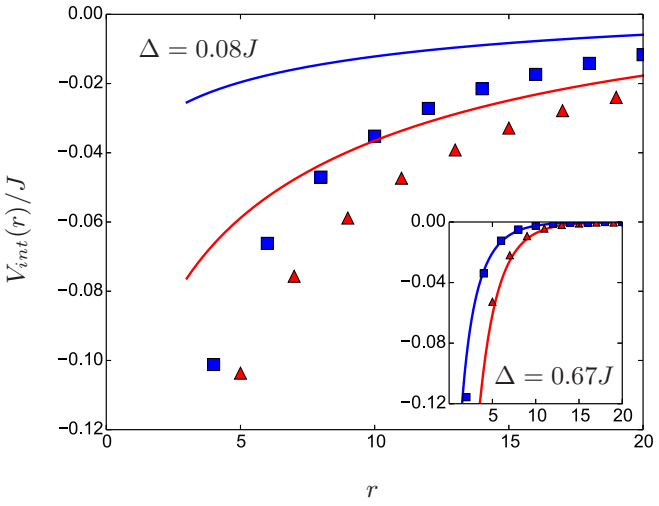

FIG. 11. (Color online) Interaction energy of two holes $V_{\rm int}(r)$ at finite magnon gaps as a function of interhole distance r. Red trangles and blue squares show the results of the Lamb-shift technique in singlet and triplet states. Red and blue solid lines represent the theoretical prediction from one-magnon exchange mechanism (21) for singlet and triplet channels. The main plot corresponds to small magnon gap ($\Delta = 0.08J$), the inset corresponds to a large magnon gap ($\Delta = 0.67J$).

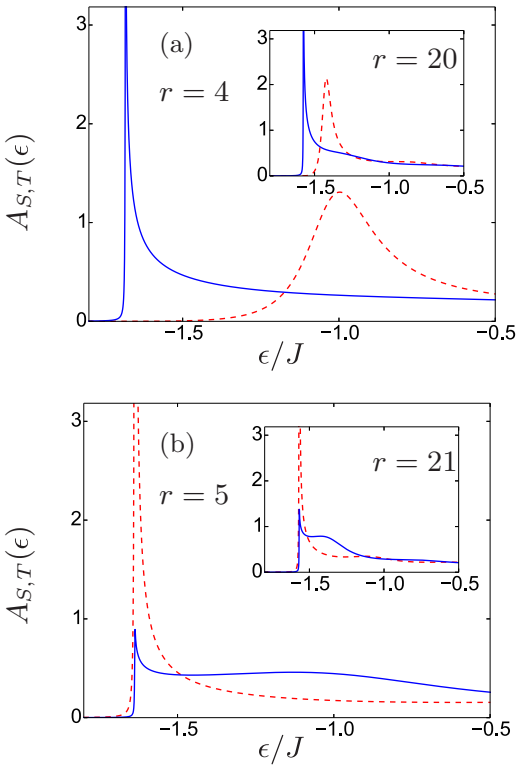

FIG. 12. (Color online) Spectral functions $A_S(\epsilon)$, $A_T(\epsilon)$ of double-fermion Green's functions in singlet and triplet channels at the QCP ($\Delta = 0$). In (a), the main plot corresponds to interhole distance $r = 4$, the inset plot to $r = 20$. In (b), the main plot corresponds to $r = 5$, the inset plot corresponds to $r = 21$. Red solid lines show a singlet state and blue dashed lines show a triplet state.

technique and the single-magnon exchange potential (21). The single-magnon exchange approximation fails in the vicinity of the QCP.

Let us now consider the most interesting case of pairing between fermions at the QCP ($\Delta = 0$). As in the case of a single fermion at the QCP, the Green's functions $G_S(\epsilon)$ and $G_T(\epsilon)$ have just power-law cuts, instead of quasiparticle peaks, with a branching point $E = E(r)$, see Figs. 12(a) and 12(b). The position $E(r)$ of the branching point gives the ground-state energy of the system. The spin channel of the ground state is specified by the spin state in which the Green's function is singular at $E(r)$. The state, in which the Green's function is not singular, corresponds to a decaying state. The imaginary part of both singlet and triplet Green's functions emerges at the same branching point $E(r)$ for any fixed r (see Fig. 12). This is due to transitions between the states with emission of soft magnons with $\omega_q \to 0$. In Fig. 12(b), we see a distinct discontinuity of both singlet and triplet spectral functions at the same branching point $E(r)$. In Fig. 12(a), the branching points also coincide, but a singlet spectral function has small spectral weight in the vicinity of the branching point.

Our results for the interaction energy $V_{\rm int}(r)$ at the QCP as a function of distance r, obtained within the Lamb-shift technique, are presented in Fig. 13. We see from the data that the interaction between two fermions is attractive, when the parity P_r is negative (positive), see Fig. 6. The binding

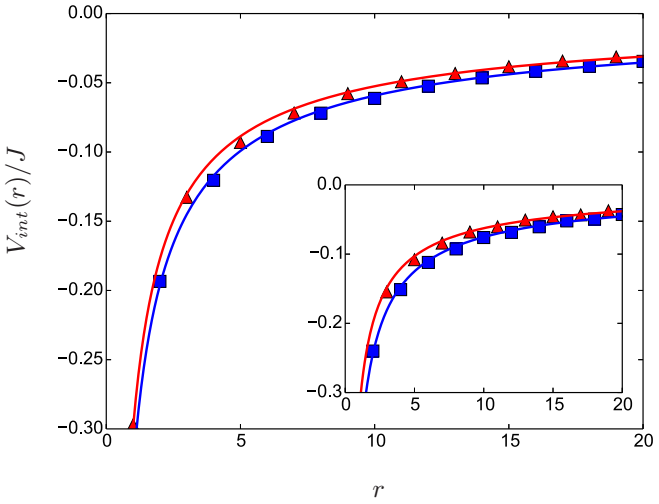

FIG. 13. (Color online) Interaction energy $V_{\rm int}(r)$ of two holes at the QCP, $\Delta = 0$. Red trangles and blue squares show the results of the Lamb-shift technique for singlet and triplet states. Red and blue solid lines represent power-law fits $V_{\rm int}(r) = -a/r^{\alpha}$ for singlet and triplet channels. The main plot corresponds to SCBA, in the inset, we represent $V_{\rm int}(r)$, which includes the first $1/\mathcal{N}$ correction to the SCBA. The exponent for all curves is approximately $\alpha \approx 0.75$.

becomes stronger at smaller interfermion distances r. The interaction energy has a power-law form:

$$V_{\rm int}(r) = -a/r^{\alpha}, \quad \alpha \approx 0.75 \tag{34}$$

with prefactor $a \approx 0.3J$, where α and a are found from the least-square fit of our numerical data. The values for prefactor a and power exponent α are slightly different for the singlet ($a = 0.3J, \alpha = 0.76$) and triplet ($a = 0.33J, \alpha = 0.74$) cases. The variations of the values of a and α are negligible within the accuracy of our calculations.

In the inset in Fig. 13, we show $V_{\rm int}(r)$, which includes vertex corrections to SCBA (31). Leading in $1/\mathcal{N}$ corrections for the singlet and triplet self-energy $\delta\Sigma_S$ and $\delta\Sigma_T$ are presented in Appendix [see diagrams in Fig. 14 and formulas (A1) and (A2)]. These corrections increase binding by about 20%, leaving the critical index α almost unchanged. Thus we conclude that corrections in $1/\mathcal{N}$ to SCBA do not change the qualitative and quantitative picture, given by SCBA.

From our calculations, we observe a very strong long-range attraction between fermions in the vicinity of the QCP. We clearly see that one magnon exchange contribution to the interaction energy vanishes at the QCP. On the contrary, accounting for multimagnon exchange processes, we obtain significant binding in singlet and triplet channels. We calculate the attraction energy due to multimagnon exchange processes as a Lamb shift of energy of a two-fermion atom due to emission of multiple magnons. The fermions interact, sharing a common bag of magnetic fluctuations and reducing the energy of fluctuations inside of the bag. Therefore the physics of interfermion attraction in the vicinity of the QCP is due to the Casimir bag mechanism.

C. Influence of mobility of fermions

How the mobility of fermions influences the considered mechanism? We do not have a full answer to this question yet. However, we do understand that the mobility does not influence the Casimir bag mechanism as soon as the fermion hopping amplitude is sufficiently small. The fermion hopping influences the dynamics in two ways: (i) it leads to additional terms in the fermion-magnon vertices (15) and (26) and (ii) hopping leads to a fermionic kinetic term in the Hamiltonian (18).

(i) The hole-magnon vertex with account of hoppings has been calculated in Ref. [16]. An important point is that the hopping induced term in the vertex has an additional power of the momentum transfer compared to the term considered in the present work. Therefore the hopping induced term is infrared irrelevant and hence, as it has been demonstrated in Ref. [16], hopping does not influence the spin-charge separation at the QCP. For the same reason, the hopping induced term in the vertex does not influence the magnon bag Casimir attraction.

(ii) The kinetic energy of the fermions, which is quadratic in the momentum of the fermion, is suppressed at small momenta comparing to the linear magnon kinetic term, and therefore is negligible at the QCP [16,39]. However, the fermion mobility imposes limitations on the time formation of the magnon bag. To address this issue, we distinguish the nearest-neighbor hopping t and the next-nearest-neighbor hopping t'. The hopping t leads to mixing between singlet and triplet pairing channels and therefore the effect of this hopping requires a special analysis. However, the hopping t' does not lead to such mixing. Therefore, in a model with the following hopping parameters, $t = 0, t' \neq 0$, and with hopping less then the depth of the potential $V_{\rm int}(r)$: $t' < 0.3J$, the binding problem is very simple. One has to solve the Lippmann-Schwinger equation with a kinetic energy due to t' and with the attraction given by Eq. (34). Obviously, the solution gives a strong binding. Of course, the set of parameters, $t = 0$, $t' \neq 0$, and $t' < 0.3J$, is not the most physically interesting one. However, the example demonstrates that in principle the mobility is consistent with the Casimir bag mechanism.

IV. CONCLUSIONS

In conclusion, we considered the interaction between two spin-1/2 fermions embedded in a two-dimensional antiferromagnetic system at the QCP, which separates ordered and disordered magnetic phases. As a model system we study a bilayer antiferromagnet at $T = 0$ with two injected holes, in which magnetic criticality is driven by interlayer coupling. We have shown that in the vicinity of the QCP the interaction between fermions can not be described by simple one-magnon exchange, unlike the case when the system is away from the QCP. The interaction mechanism is similar to the Casimir effect and is due to multimagnon exchange processes. To incorporate features of Casimir physics, we developed an approach, which we call a Lamb-shift technique. We considered a composite two-fermion atom and calculated its energy shift (Lamb shift) provided by radiation of magnons. We found strong attraction between the fermions in spin singlet and triplet states depending on the parity of the interfermion

distance r, which is positive (negative) for even (odd) r. Positive (negative) parity corresponds to attraction in triplet (singlet) channel. The attractive potential has a power-law form $V_{\rm int}(r) \propto -1/r^{\alpha}$ with the exponent $\alpha \approx 0.75$.

We suppose that our work sheds light on the influence of magnetic criticality on fermion pairing mediated by magnons. We also believe that our results are conceptually applicable to cuprates.

ACKNOWLEDGMENTS

We gratefully acknowledge A. Chubukov, G. Khaliullin, and I. Terekhov for useful discussions. This research was supported by Australian Research Council (Grant No. DP110102123).

APPENDIX: LEADING $1/\mathcal{N}$ CORRECTIONS TO SCBA FOR TWO-FERMION GREEN'S FUNCTION

Let us consider $1/\mathcal{N}$ corrections to the self-energies $\Sigma_S(\epsilon)$ and $\Sigma_T(\epsilon)$, calculated in self-consistent Born approximation [see Eq. (31)]. In order to do this, we account for vertex corrections $\delta\Sigma_S(\epsilon)$ and $\delta\Sigma_T(\epsilon)$ to self-energies obtained in SCBA, the corresponding diagrams are shown in Fig. 14. The vertex correction to the singlet self-energy reads

$$\delta\Sigma_S(\epsilon) = 3\sum_{\boldsymbol{q},\boldsymbol{k}} |g_{ST}(q)|^2 |g_{ST}(k)|^2 G_{T,q} G_{T,k} G_{S,qk} - 6\sum_{\boldsymbol{q},\boldsymbol{k}} g_{ST}(q) g^*_{ST}(k) g_{TT}(k) g^*_{TT}(q) \times G_{T,q} G_{T,k} G_{T,qk}. \quad \text{(A1)}$$

The combinator factors come from contractions of the corresponding tensor structures of the effective vertices in Eq. (25).

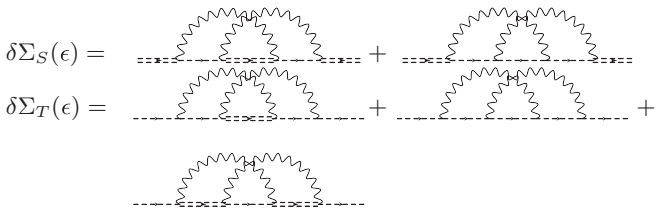

FIG. 14. Diagrams for the leading $1/\mathcal{N}$ corrections $\delta\Sigma_S(\epsilon)$ and $\delta\Sigma_T(\epsilon)$ (a) to singlet and (b) to triplet self-energies. Double dashed line and dashed line represent two-fermion Green's functions in the singlet and triplet channels, respectively.

In a similar way, the vertex correction to the triplet self-energy is given by

$$\delta\Sigma_T(\epsilon) = \sum_{\boldsymbol{q},\boldsymbol{k}} |g_{ST}(q)|^2 |g_{ST}(k)|^2 G_{S,q} G_{S,k} G_{T,qk} - 2\sum_{\boldsymbol{q},\boldsymbol{k}} g_{TT}(q) g^*_{ST}(k) g^*_{ST}(q) g_{ST}(k) G_{T,q} G_{T,k} G_{S,qk} + 2\sum_{\boldsymbol{q},\boldsymbol{k}} |g_{TT}(q)|^2 |g_{TT}(k)|^2 G_{T,q} G_{T,k} G_{T,qk}. \quad \text{(A2)}$$

Here, we are using shorten notations $G_{n,q} = G_n(\epsilon - \omega_q)$, $G_{n,k} = G_n(\epsilon - \omega_k)$, and $G_{n,qk} = G_n(\epsilon - \omega_q - \omega_k)$ for the singlet and triplet Green's functions ($n = S, T$). One can check that in the limit $r \to \infty$, the correction $\delta\Sigma_S$ will be suppressed by the factor $1/\mathcal{N} = 1/3$ with respect to $\Sigma^{(2\,\text{loop})}_{S,T}$ calculated in SCBA within a two-loop approximation.

The relative shift of binding energy, calculated with and without vertex correction, does not exceed 20%. It can be considered as a confirmation of applicability of the $1/\mathcal{N}$ expansion for the effective Lamb-shift theory described by the Hamiltonian (25).

[1] M. A. Hossain, J. D. F. Mottershead, D. Fournier, A. Bostwick, J. L. McChesney, E. Rotenberg, R. Liang, W. N. Hardy, G. A. Sawatzky, I. S. Elfimov, D. A. Bonn, and A. Damascelli, Nat. Phys. **4**, 527 (2008).
[2] R.-H. He *et al.*, New J. Phys. **13**, 013031 (2011).
[3] H.-B. Yang, J. D. Rameau, Z.-H. Pan, G. D. Gu, P. D. Johnson, H. Claus, D. G. Hinks, and T. E. Kidd, Phys. Rev. Lett. **107**, 047003 (2011).
[4] N. Doiron-Leyraud, C. Proust, D. LeBoeuf, J. Levallois, J. B. Bonnemaison, R. Liang, D. A. Bonn, W. N. Hardy, and L. Taillefer, Nature (London) **447**, 565 (2007).
[5] B. Vignolle, A. Carrington, R. A. Cooper, M. M. J. French, A. P. Mackenzie, C. Jaudet, D. Vignolles, C. Proust, and N. E. Hussey, Nature (London) **455**, 952 (2008).
[6] Z. Liu and E. Manousakis, Phys. Rev. B **45**, 2425 (1992).
[7] A. I. Milstein and O. P. Sushkov, Phys. Rev. B **78**, 014501 (2008).
[8] C. Stock, W. J. L. Buyers, Z. Yamani, Z. Tun, R. J. Birgeneau, R. Liang, D. Bonn, and W. N. Hardy, Phys. Rev. B **77**, 104513 (2008).
[9] V. Hinkov, D. Haug, B. Fauqué, P. Bourges, Y. Sidis, A. Ivanov, C. Bernhard, C. T. Lin, and B. Keimer, Science **319**, 597 (2008).
[10] D. Haug, V. Hinkov, Y. Sidis, P. Bourges, N. B. Christensen, A. Ivanov, T. Keller, C. T. Lin, and B. Keimer, New J. Phys. **12**, 105006 (2010).
[11] D. J. Scalapino, Phys. Rep. **250**, 329 (1995); P. Monthoux and D. Pines, Phys. Rev. B **47**, 6069 (1993); A. Abanov, A. V. Chubukov, and J. Schmalian, Adv. Phys. **52**, 119 (2003).
[12] M. Yu. Kuchiev and O. P. Sushkov, Physica C **218**, 197 (1993); V. V. Flambaum, M. Yu. Kuchiev, and O. P. Sushkov, *ibid.* **227**, 267 (1994).
[13] Y. Wang and A. V. Chubukov, Phys. Rev. B **88**, 024516 (2013).
[14] P. Krotkov and A. V. Chubukov, Phys. Rev. Lett. **96**, 107002 (2006).
[15] E. G. Moon and S. Sachdev, Phys. Rev. B **80**, 035117 (2009).
[16] M. Holt, J. Oitmaa, W. Chen, and O. P. Sushkov, Phys. Rev. Lett. **109**, 037001 (2012); Phys. Rev. B **87**, 075109 (2013).
[17] H. B. C. Casimir and D. Polder, Phys. Rev. **73**, 360 (1948).
[18] J. R. Schrieffer, X. G. Wen, and S. C. Zhang, Phys. Rev. Lett. **60**, 944 (1988).

[19] L. P. Pryadko, S. Kivelson, and D. W. Hone, Phys. Rev. Lett. **80**, 5651 (1998).
[20] A. Chodos, R. L. Jaffe, K. Johnson, and C. B. Thorn, Phys. Rev. B **10**, 8 (1974).
[21] G. E. Brown and M. Rho, Phys. Lett. B **82**, 177 (1979).
[22] A. W. Sandvik and D. J. Scalapino, Phys. Rev. Lett. **72**, 2777 (1994).
[23] A. W. Sandvik, A. V. Chubukov, and S. Sachdev, Phys. Rev. B **51**, 16483 (1995).
[24] Z. Weihong, Phys. Rev. B **55**, 12267 (1997).
[25] V. N. Kotov, O. Sushkov, Z. Weihong, and J. Oitmaa, Phys. Rev. Lett. **80**, 5790 (1998).
[26] M. Vojta and K. W. Becker, Phys. Rev. B **60**, 15201 (1999).
[27] Y. Matsushita, M. P. Gelfand, and C. Ishii, J. Phys. Soc. Jpn **68**, 247 (1999).
[28] D. K. Yu, Q. Gu, H. T. Wang, and J. L. Shen, Phys. Rev. B **59**, 111 (1999).
[29] C. Jurecka and W. Brenig, Phys. Rev. B **63**, 094409 (2001).
[30] R. Eder, Phys. Rev. B **57**, 12832 (1998).
[31] Y. Saito, A. Koga, and N. Kawakami, J. Phys. Soc. Jpn **72**, 1208 (2003).
[32] A. V. Chubukov, JETP Lett. **47**, 129 (1989); S. Sachdev and R. N. Bhatt, Phys. Rev. B **41**, 9323 (1990).
[33] J. Zinn-Justin, *Quantum Field Theory and Critical Phenomena*, 3rd ed. (Oxford University Press, Oxford, 1996).
[34] M. Vojta, C. Buragohain, and S. Sachdev, Phys. Rev. B **61**, 15152 (2000).
[35] O. P. Sushkov, Phys. Rev. B **62**, 12135 (2000).
[36] I. E. Dzyaloshinskii, JETP **30**, 1152 (1956).
[37] A. Lüsher and O. P. Sushkov, Phys. Rev. B **71**, 064414 (2005).
[38] C. Itzykson and J.-B. Zuber, *Quantum Field Theory* (McGraw-Hill International Book, New York, 1980).
[39] S. Sachdev, M. Troyer, and M. Vojta, Phys. Rev. Lett. **86**, 2617 (2001).